1070 *Chem. Mater.* **2011,** *23,* 1070–1077
DOI:10.1021/cm1025156

CHEMISTRY OF MATERIALS
Article

Size and Morphology Control of Ultrafine Refractory Complex Oxide Crystals

Jean Yves Chane-Ching,*,† Gaetan Martinet,† Pierre Jean Panteix,† Charlotte Brochard,† Antoine Barnabé,† and Marc Airiau‡

†*CIRIMAT, Université de Toulouse, CNRS, 118, Route de Narbonne, 31062 France, and*
‡*Rhodia Recherches et Technologies, Rue de la Haie Coq, 93308 Aubervilliers, France*

Received September 2, 2010. Revised Manuscript Received November 17, 2010

High-temperature complex oxides are of considerable interest as their applications cover a broad spectrum from catalytic to optical technology. Indeed, new exciting opportunities might emerge if these high-temperature complex oxides, in which structure crystallization is achieved at temperatures $T > 1000$ °C, could be synthesized as nonaggregated, ultrafine building blocks. In general, such refractory complex oxide particles are difficult to synthesize as ultrafine crystals because of the strong driving force available for sintering and coarsening in this high-temperature range. This paper reports a new synthetic process for the preparation of nonaggregated, ultrafine barium hexa-aluminate, $BaO, 6Al_2O_3$, (BHA), and $Ba_{0.9}Eu_{0.1}MgAl_{10}O_{17}$, (BAM) crystals in which structure crystallization occurs around 1300 °C. Our process is based on the Ba^{2+} and Al^{3+} ions high-temperature controlled diffusion from carbon−inorganic hybrid compounds prepared from soft chemistry routes. Control of morphology of these refractory complex aluminates displaying nanoplatelets morphology was achieved via the tailoring of high-temperature diffusion lengths of the various cations involved in the formation of these ultrafine refractory crystals.

I. Introduction

A wide range of electrical and optical properties of oxide nanocrystals depends sensitively on chemical composition, size, and shape. Synthesis routes allowing control of morphology, size, and homodispersity of oxide nanocrystals have been largely developed using soft chemistry methods. Extensive studies on fabricating single-cation,[1,2] as well as binary or ternary oxides[3,4] involving mainly hydrothermal or solvothermal routes, have been achieved on nanocrystals in which structure crystallization occurs at relatively low temperatures, $T < 500$ °C. In contrast, a limited amount of work has contributed to the manufacture of complex oxide nanocrystals displaying structures such as spinel, garnet,[5]and β-alumina type[6] in which structure crystallization is performed in the high-temperature range, $T > 1000$ °C. In particular, $BaAl_{12}O_{19}$, (barium hexa-aluminate, BHA), $Ba_{0.9}Eu_{0.1}MgAl_{10}O_{17}$, (BAM), $SrAl_2O_4:Eu^{2+}:Dy^{3+}$, (SAO), or doped $Y_3Al_5O_{12}$ (YAG) materials have many important properties and applications in science and engineering such as catalysis,[7,8] luminescence,[9,10] phosphorescence[11], or opto-electronics. Indeed, more applications and new functional materials might emerge if these high-temperature oxides with chemical compositions of higher complexity could be synthesized as nonaggregated, ultrafine particles. For optical applications, formation of nonaggregated, ultrafine BAM or SAO crystals possessing mean particle size lower than 300 nm is highly desired for the fabrication of transparent optical, luminescent[12], or phosphorescent devices. For catalytic application, preparation of high-temperature, complex oxide, ultrafine crystals with controlled morphology could serve as a key development toward achieving very high-temperature stable catalyic materials. For instance, the benefit of high-temperature complex oxide nanocrystals displaying controlled morphology is illustrated through anisotropic diffusion of atoms in the $Ba-\beta-Al_2O_3$ structure. The anisotropic morphology contributes to an increased resistance to crystal growth along the *c* axis and inhibits sintering, thus improving their catalytic performances. In general, such nonaggregated, ultrafine, refractory,

*E-mail: chane@chimie.ups-tlse.fr.

(1) Chatry, M.; Henry, M.; In, M.; Sanchez, C.; Livage, J. *J. Sol−Gel Sci. Technol.* **1994**, *1*, 233.
(2) Idrissi-Kandri, N.; Ayral, A.; Guizard, C.; El Ghadraoui, H.; Cot, L. *Mater. Lett.* **1999**, *40*, 52.
(3) Deshpande., A. S.; Pinna, N.; Beato, P.; Antonietti, M.; Niederberger, M. *Chem. Mater.* **2004**, *16*, 2599.
(4) Garnweitner, G.; Nierderberger, M. *J. Am. Ceram. Soc.* **2006**, *89*, 1801.
(5) Sun, Z.; Yuan, D.; Duan, X.; Wei, X.; Sun, H.; Luan, C.; Wang, Z.; Shi, X.; Xu, D.; Lu, M. *J. Cryst. Growth* **2004**, *260*(1−2), 171.
(6) Kang, Y. C.; Chung, Y. S.; Park, S. B. *J. Mater. Sci. Lett.* **1999**, *18*, 779.
(7) Gaillard, F.; Artizzu, P.; Brulle, Y.; Primet, M. *Surf. Interface Anal.* **1998**, *26*, 367.
(8) Groppi, G.; Assandri, F.; Bellotto, M.; Cristiani, C.; Forzatti, P. *J. Solid State Chem.* **1995**, *114*, 326.
(9) Kuo, K. T.; Lee, S. P.; Chen, S. Y.; Cheng, B. M.; Lu, C. C.; Ting, H. C. *J. Phys. Chem. Solids* **2008**, *69*, 362.
(10) Lee, D. L.; Lee, S. M.; Byun, Y.; Lee, E. S.; Bae, J. Y. *J. Appl. Polym. Sci.* **2008**, *108*, 2571.
(11) Qiu, Z.; Zhou, Y.; Lue, M.; Zhang, A.; Ma, Q. *Solid State Sci.* **2008**, *10*(5), 629.
(12) Watchi, M. I.; Duran, M.; Huignard, A. Patent WO 001872, 2005.

Published on Web 01/05/2011

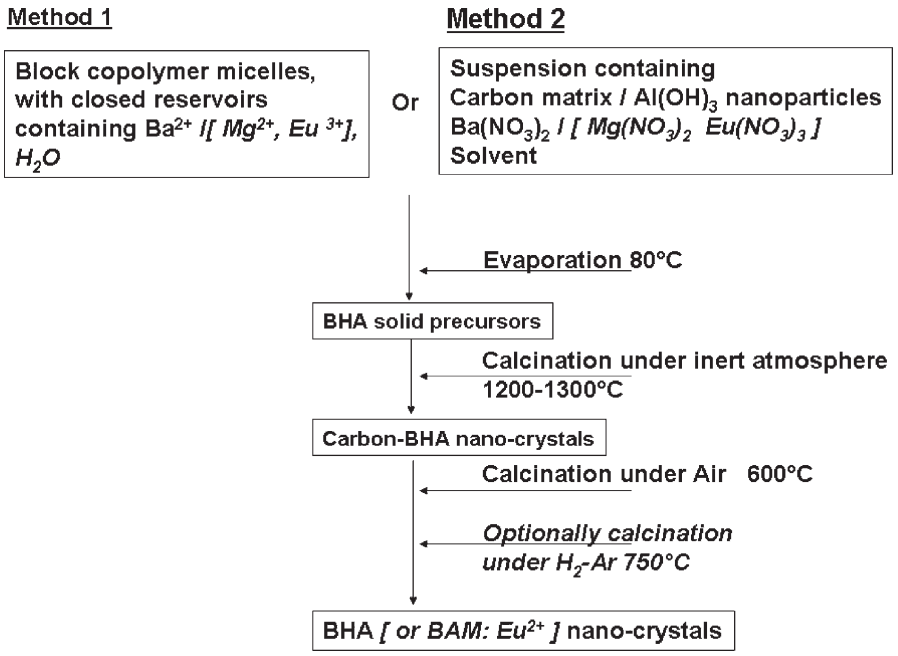

Figure 1. Diagrams of the copolymer micelles route and of the carbon matrix-mediated processing of barium hexa aluminate BHA (or BAM:Eu) ultrafine crystals. Structure crystallization of the BHA (or BAM Eu) is achieved by heat treatment of BHA (or BAM:Eu) precursors at 1200−1300 °C under inert atmosphere. Ultrafine, pure BAM (or BAM:Eu) crystals are formed from pyrolysis of the high surface area carbon matrix via air calcination performed at 600 °C.

complex oxide particles are difficult to synthesize because of the strong driving force available for sintering and coarsening. Indeed, fabrication of these nonaggregated, ultrafine complex oxide crystals with controlled size and morphology remains a great scientific challenge because of the difficulty of controlling nucleation−growth regimes in this high-temperature range. Previous research works describing the synthesis of these ultrafine high-temperature complex oxide crystals are based on high-temperature routes such as combustion[13,14] or process spray pyrolysis.[15,16] The first interesting results involving spray pyrolysis[15] have been recently reported on the production of nonaggregated SAO spherical nanosized powders. Indeed, this process is based on a quench of solvent droplets containing the metallic cations at high temperature but do not allow any control of crystal morphology. Because size and morphology control has been largely reported using soft chemistry routes in the case of the fabrication of low-temperature oxides, innovative processes combining soft chemistry routes with an appropriate high-temperature calcination step are thus highly desired with the objective to fabricate the nonaggregated, ultrafine refractory oxide crystals. In this context, the first attractive route previously reported to the fabrication of complex oxide nanocrystals is the citrate sol−gel method[17,18], utilizing the strong chemical complex between metal cations and citrates, leading to fine and homogeneous powders with controlled stoichiometry. The second approach involves the use of reverse microemulsion droplets as nanoreactors.[19−21] Unfortunately, these processes yield nanosized crystals but without any well-defined morphology. Moreover, these nanocrystals were aggregated in accordance with the large driving force for solid diffusion at these high temperatures.

Here, we report new synthetic routes for the preparation of ultrafine, nonaggregated barium hexa-aluminate, $BaO,6Al_2O_3$, (BHA) and doped barium magnesium hexa-aluminate $Ba_{0.9}Eu_{0.1}MgAl_{10}O_{17}$, (BAM) crystals in which structure crystallization occurs around 1300 °C. Our procedure includes as the first step, the formation at low temperature of a BHA (or BAM) precursor using aqueous soft chemistry procedures and possessing a well-defined distribution of the metallic cations (Al^{3+}, Ba^{2+}, and optionally Mg^{2+}, Eu^{3+}). Two different distributions of the metallic cations were investigated (Figure 1). In the first method, BHA precursors were prepared using double hydrophilic block copolymer micelles acting as closed reservoirs of the various metallic ions. In the second method, BHA (or BAM) precursors are composed of 4 nm $Al(OH)_3$ colloids acting as nanoreactors homogeneously dispersed onto a high surface area carbon matrix in which the metallic cations (Ba^{2+} and optionally Mg^{2+}, Eu^{3+}) are homogeneously distributed. For the two methods, BHA (or BAM) structure crystallization is obtained in the second step, performed at high temperature. Growth

(13) Yu, X.; Zhou, C.; He, X.; Peng, Z.; Yang, S. *Mater. Lett.* **2004**, *58* (6), 1087.
(14) Chander, H.; Haranath, D.; Shanker, V.; Sharma, P. *J. Cryst. Growth* **2004**, *271*(1−2), 307.
(15) Li, C.; Imai, Y.; Adachi, Y.; Yamada, H.; Nishikubo, K.; Xu, C. *J. Am. Ceram. Soc.* **2007**, *90*(7), 2273.
(16) Jung, K. Y.; Kang, Y. C. *Mater. Lett.* **2004**, *58*(16), 2161.
(17) Kim, D. K.; Hwang, S. H.; Kim, I. G.; Park, J. C.; Byeon, S. H. *J. Solid State Chem.* **2005**, *178*, 1414.
(18) Singh, R.; Khardekar, R. K.; Kumar, A.; Kohli, D. K. *Mater. Lett.* **2007**, *61*(3), 921.
(19) Zarur, A. J.; Ying, J. Y. *Nature* **2000**, *403*, 65.
(20) Wang, Y. H.; Li, F. *J. Lumin.* **2007**, *122−123*, 866.
(21) Teng, F.; Tian, Z.; Xu, J.; Xiong, G.; Lin, L. *Stud. Surf. Sci. Catal.* **2004**, *147*, 493.

inhibition of the BHA (or BAM) crystals is achieved through high-temperature controlled diffusion of the metal cations under inert atmosphere into the initial or in situ-formed high surface area carbon matrix. Individual ultrafine BHA (or BAM) crystals were further collected under subsequent pyrolysis of the transient carbon matrix performed under air but at a much lower temperature (600 °C), thus minimizing interparticle aggregation. A key parameter controlling ion diffusion and growth of the BHA (or BAM) crystals occurring during the high-temperature heat treatment under inert atmosphere of the carbon−BHA precursor mixtures is the BHA volume fraction $\Phi_{v\mathrm{BHA}}$, $\Phi_{V\ \mathrm{BHA}}$= [Volume BHA] /[(Volume BHA) + (Volume carbon)].

II. Experimental Section

II.1. Preparation of Ultrafine BHA (or BAM) Particles. *BHA Precursors Involving Double Hydrophilic Block Copolymer Micelles*. (*Method 1*). $Ba(NO_3)_2$ and $Al(NO_3)_3$ 9 H_2O were purchased from Fluka. Formation of colloidal micellar nanoassemblies was investigated from a series of PAA homopolymer−PAA-b-PAM copolymer compositions. Homopolymer PAA, M_w = 2000 g/mol, was purchased from Fluka, and the double hydrophilic block copolymer poly(acrylic acid)−polyacrylamide), PAA-b-PAM, PAA = 3600 g/mol, PAM = 8000 g/mol was obtained from Rhodia, Aubervilliers, France. Various compositions were investigated with x = [PAA-b-PAM]/([PAA] + [PAA-b-PAM]), with x ranging from x = 0 to x = 1 and with r = [AA]/([Al]+[Ba]) mol, with r ranging from 1 to 2.5. The various aluminum cations investigated (Al^{3+}, $AlOH^{2+}$, or $Al_{13}{}^{7+}$) were synthesized from $Al(NO_3)_3$ 9 H_2O.

In a typical experiment, ($Al_{13}{}^{7+}$−Ba^{2+}−PAA-PAM, x = 1, $\Phi_{v\mathrm{BHA}}$ = 0.025, r = 2), 250 cm^3 of PAA-b-PAM solution were prepared by dissolving 6.96 g of PAA-PAM copolymer in deionized water, adjusted at pH 8. The PAA-b-PAM solution was added to 250 cm^3 of inorganic precursor stock solution containing $Al_{13}{}^{7+}$ and Ba^{2+}. After stirring at 25 °C during 48 h, removal of the free Al^{x+} and Ba^{2+} was performed by ultrafiltration. The required equivalent volume fraction of BHA, $\Phi_{v\mathrm{BHA}}$ = 0.025 was obtained by adding 12 g of polyvinyl pyrolidone, PVP = 10000 g/mol, to the PAA-b-PAM−Ba^{2+}−$Al_{13}{}^{7+}$ mixture. Solid powders formed from copolymer micelles containing mineralized cores were collected after drying by evaporation at 80 °C in an oven.

BHA Precursors Involving Distributions of $Al(OH)_3$ Colloids and Ba^{2+} Cations onto a High Surface Area Matrix. (*Method 2*). A 4 nm $Al(OH)_3$ colloidal dispersion containing Ba^{2+} was prepared following a procedure previously described[2] for the synthesis of $Al(OH)_3$ colloids, except for the addition of $Ba(NO_3)_2$ before the formation of the hydroxide gel by urea decomposition. A Ba/Al molar ratio of 0.095 was determined on the Ba^{2+}−$Al(OH)_3$ dispersion after peptization of the hydroxide gel at pH 4.5 using diluted HNO_3 and subsequent purification by ultrafiltration. Discrete, ultrafine BHA crystals were prepared from mixtures containing high surface area carbon (PICACTIF BP 10, 2300 m^2/g) and the Ba^{2+}−$Al(OH)_3$ dispersion. In a typical experiment, (Ba/Al = 0.095, Φv_{BHA} = 0.0375), 6 g carbon (PICACTIF BP 10) was dispersed into 40 mL of H_2O. To this suspension adjusted to pH 4.5, 10.4 mL Ba^{2+}−$Al(OH)_3$ colloidal dispersion (Al = 0.9 M, Ba−Al = 0.095, pH 4.5), was added. The resulting suspensions were stirred during 16 h at 20 °C in order to disperse the Ba^{2+} and $Al(OH)_3$ nanoparticles onto the high surface area carbon matrix. Carbon−BHA solid precursors were obtained by slow evaporation of the suspensions in an oven at 80 °C.

BHA Structure Crystallization and Discrete, Ultrafine BHA Crystals Formation. BHA solid precursors formed from copolymer micelles containing mineralized cores (method 1) or from evaporation of the carbon−$Al(OH)_3$−Ba^{2+} suspensions (method 2) were calcined for BHA structure crystallization under Ar atmosphere, respectively, at 1250 °C/12 h or 1300 °C/4 h. A subsequent air calcination step was performed at 600 °C for 2 h in order to pyrolyse the carbon. TGA studies provide evidence for the complete removal of carbon. In some cases, in order to improve the individualization of the ultrafine crystals, the BHA crystals were subjected to ball milling during 1 h using 0.3 mm Al_2O_3 balls.

Transposition to Ultrafine BAM Crystals Preparation. $Mg(NO_3)_3$ et $Eu(NO_3)_3$ were purchased from Fluka. Ultrafine BAM:Eu^{2+} crystals were synthesized using the procedure of method 2 except for the addition of $Eu(NO_3)_3$ and $Mg(NO_3)_2$ in the required concentrations to form Eu^{3+}−Mg^{2+}−Ba^{2+}−$Al(OH)_3$ colloids. Respective molar ratios of Ba/Al = 0.11, Mg/Al=0.10, and Eu/Al=0.08 were achieved after peptization using HNO_3 and subsequent purification by ultrafiltration for the concentrated aqueous dispersion. The suspensions containing the high surface area carbon and the (Eu^{3+}−Mg^{2+}−Ba^{2+}−$Al(OH)_3$) colloids were prepared in an hydro alcoholic medium, $(EtOH:H_2O)=(50:50)_{vol}$, and the solvent was further eliminated by rotoevaporation at 80 °C. In a typical experiment, 6 g of carbon was mixed to 6.75 mL of Ba^{2+}−Eu^{3+}−Mg^{2+}−$Al(OH)_3$ colloidal dispersion (Φv_{BAM} = 0.025). In order to achieve the BAM structure crystallization, calcination of the carbon−BAM precursors was carried out at 1250 °C for 4 h under argon. The Eu^{3+}→Eu^{2+} reduction was achieved through an additional heat treatment under Ar, 3.9% H_2 at 750 °C for 2 h after the 600 °C for 2 h air calcination step.

II.2. Characterization. SAXS experiments were conducted on beamline ID02 at ESRF, Grenoble. Dispersions were introduced in cylindrical cells with diameters of 24 mm and thicknesses of 2 mm, limited by two mica windows. Incident wavelength was 0.995 Å. SAXS patterns were collected on a CCD detector with sample-to-detector distance of 1.5 m. SAXS data underwent radial averaging and background correction, taking into account scattering from the two mica windows and scattering by the solvent. Transmission electron microscopy (TEM) was performed on a Jeol Jem 2100F with an accelerating voltage of 200 kV, equipped with an energy dispersive spectrometer EDS (probe surface of 7.0 nm x 7.0 nm). Cryo-TEM images were recorded from samples without any dilution. A small volume of sample (6−7 μL) was deposited onto a lacey carbon membrane supported on TEM copper grids. The grid was frozen at high speed in liquid ethane on a benchtop setup. After this freezing step, grids were maintained at low temperature in liquid nitrogen, then transferred onto a cold sample holder and observed in a JEOL 1200 EX TEM microscope, using low-dose configuration. Observations were made at a magnification of 20000, and images were recorded on conventional photographic films. The crystal structure refinement was based on X-ray powder diffraction data. The powder pattern was collected using a diffracted beam monochromator (Philipps vertical diffractometer PW 1050-70). The refinement was performed using a Rietveld method and a general structure analyzer system GSAS.

III. Results and Discussion

III.1. Synthesis of Ultrafine BHA Particles Formed from Double Hydrophilic Copolymer Micelles. *BHA*

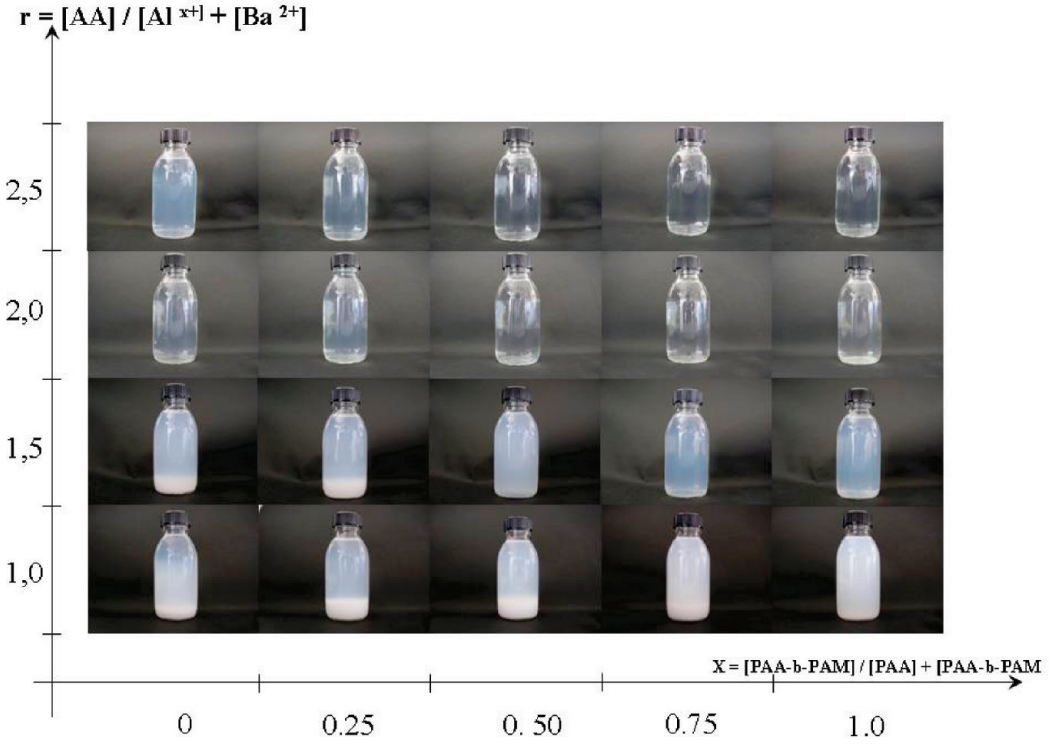

Figure 2. Influence of metal complexation on the formation of colloidal dispersions in the "Al_{13}^{7+}– Ba^{2+}–PAA–PAA-b-PAM" system. Colloidal nanoassemblies are formed in a large range of homopolymer–copolymer mixtures for $r \geq 2$, r = [AA]/([Al]+[Ba]) mol.

Precursor. Copolymer-based nanoassemblies containing Al^{3+} and Ba^{2+} cations in BHA stoichiometric ratio were first designed using poly(acrylic acid) homopolymer or poly(acrylic acid)–b-polyacrylamide, double hydrophilic block copolymer, or their mixtures. Because the Ba^{2+} and Al^{3+} cations are known to display different reactivity toward hydroxide or carbonate solid formation via OH^- or CO_3^{2-} precipitation, the PAA oligomer offer the advantage to yield spontaneous coordination of both the barium and aluminum cations. In order to optimize nanoscale homogeneous coprecipitation of the aluminum and barium cations, various aluminum cations (Al^{3+}, $Al(OH)_2^+$, Al_{13}^{7+}) exhibiting various reactivity toward the acrylate group were investigated. Solutions of containing block copolymer and homopolymer were prepared by simple dissolution in deionized water, and pH of the solutions were preadjusted to 8 before mixing with solution of inorganic precursors. After mixing, the pH of the suspensions was readjusted at pH 8 in order to achieve a very high degree of dissociation of the acrylic acid groups and hydrolysis of the aluminum cation in the micellar nanoassemblies.

A critical parameter for the formation of colloidal nanoassemblies previously reported for inorganic ions, copolymer nanoassemblies, is the metal complexation by acrylate groups, expressed as the number of acrylate groups per metal atom, r = [AA]/[M^{x+}].[22–24] Investigation of colloidal nanoassemblies by varying r = [AA]/[Al^{3+} + Ba^{2+}] for nanoassemblies prepared in the system "PAA–PAA-b-PAM/Ba^{2+}–Al^{x+}" at various homopolymer–copolymer ratios, x = [PAA-b-PAM]/[PAA-b-PAM + PAA] showed the formation of colloidal nanoassemblies in a large range of homopolymer–copolymer mixtures for $r \geq 2$ (Figure 2). Selective binding of the Al^{x+} and Ba^{2+} cations into the micellar nanoassemblies was demonstrated by chemical analysis of the Ba^{2+} and Al^{x+} cations in the ultrafiltrates after ultrafiltration of the colloidal suspensions on 3 kDa membranes. Best results were obtained with suspensions involving Al_{13}^{7+} cations, resulting in coordination of both the Ba^{2+} and Al_{13}^{7+} cations inside the micellar nanoassemblies up to 90% atom. Colloidal nanoassemblies synthesized using Al_{13}^{7+} and Ba^{2+} were fully characterized by cryo-TEM and small-angle X-ray scattering (SAXS). Cryo-TEM images of colloidal nanoassemblies prepared at $r = 2$, $x = 0$, 0.5, and 1 reveals nanoparticles perfectly dispersed. Size of the micellar nanoassemblies was observed to be on the order of 5 nm, although their dimensions are close to the resolution limit of cryo-TEM micrographs. Nevertheless, for suspensions prepared at $x = 0$ and 0.5, some aggregates could be observed. Figure 3 shows the SAXS patterns of nanoassemblies prepared in the system "PAA–PAA-b-PAM/Ba^{2+}–Al_{13}^{7+}" at various copolymer–homopolymer ratios, x. SAXS curves recorded from these transparent colloidal dispersions exhibit two regimes, one first regime at low-wave vector q with a moderate decrease in intensity, and a second regime at higher q values with a stronger decrease in intensity. From the various scattering curves, a lower decrease in intensity in

(22) Gerardin, C.; Sanson, N.; Bouyer, F.; Fajula, F.; Putaux, J. L.; Joanicot, M.; Chopin, T. *Angew. Chem., Int. Ed.* **2003**, *42*, 3681.
(23) Bouyer, F.; Sanson, N.; Destarac, M.; Gerardin, C. *New J. Chem.* **2006**, *30*, 399.
(24) Qi, L.; Coelfen, H.; Antonietti, M. *Chem. Mater.* **2000**, *12*, 2392.

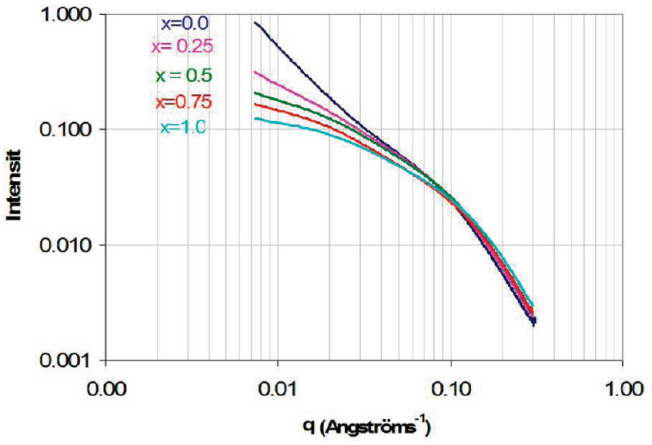

Figure 3. SAXS patterns of the nanoassemblies formed in the "Al_{13}^{7+}−Ba^{2+}−PAA−PAA-b-PAM" system showing a less aggregated system observed for the colloidal dispersion prepared with 100% block copolymer, $x = 1$.

the first regime and corresponding to the less aggregated system is observed for the colloidal dispersion prepared with 100% block copolymer, $x = 1$. At high q value, the high q slope is close to a q^{-3} behavior, which is attributed to the presence of porosity in the particles, a rough interface, or the contribution of scattering from the corona of homopolymer−copolymer chains. Quantitative data can be extracted by considering a two-scale model of aggregated particles, such as the model developed by G. Beaucage.[25,26] This model is based on the assumption of primary particles, aggregated in semifractal structures with finite extension in real space. For the colloidal dispersion prepared at $x = 1$, simulation yields a radius of gyration of nanoparticles of 3 nm and a pseudofractal dimension of 0.74. This latter value lower than 1 means that the aggregation is only partial and that the discrete nanoparticles were associated with few aggregates as observed on the cryo-TEM images of the as-synthesized nanoassemblies. All these observations highlight that our suspensions formed using Al_{13}^{7+} and block copolymer, $x = 1$, are the less aggregated.

Our synthetic method includes after evaporation−drying of the colloidal micellar nanoassemblies a calcination step performed in inert atmosphere at high temperature ($T > 1200$ °C), transforming the PAA-b-PAM block copolymer into carbon foam-yielding BHA crystals−carbon mixtures. Another advantage of use of block copolymer suspensions, $x = 1$, is the achievement of a highly homogeneous distribution of nanosized inorganic cores originated from the preformed micellar nanoassemblies into the carbon foam. Indeed, the high interactions existing between the complexing PAA moiety or homopolymer and the nanosized inorganic hydroxide cores enables retention of their dispersion, particularly at temperatures at which fusion of the homopolymer or copolymer occurs during the heat treatment. Optimum dispersion of the BHA crystals into the carbon foam occurs for the highest concentration of peripheral PAM stabilizing moieties achieved with block copolymer suspensions, $x = 1$.

BHA Structure Crystallization and Preparation of Individual, Ultrafine BHA Particles. To control BHA crystal size formed from the inorganic−carbon mixtures, synthesis parameters such as Φ_{BHA}, calcination temperature, and duration were carefully investigated. Lower BHA volume fraction, Φv_{BHA}, of the BHA−carbon mixtures results in an increase in the BHA onset crystallization temperature. Another illustration of the inhibition of BHA crystal growth by carbon is the dependence of the primary crystallite size, determined using the Scherrer relation and the simplified Williamson−Hall plot, on the Φv_{BHA}. In the range of $0.025 < \Phi v_{BHA} < 0.075$, lower Φv_{BHA} values result in smaller primary crystal size. Thus, for products synthesized in the "PAA-b-PAM−Ba^{2+}−Al_{13}^{7+}" system, $x = 1$, $r = 2$, and $(Ba/Al)_{mol} = 0.083$, the smallest primary crystallite size of around 200 nm of highly pure BHA crystals embedded in carbon were obtained at $\Phi v_{BHA} = 0.025$, after calcination at 1250 °C for 12 h. Although our chemical analysis results indicate composition of barium and aluminum ions within the 5 nm nanoassemblies in the stoichiometric ratio, the BHA structure crystallization of the hydroxide precursors in the carbon occurs at a relatively high temperature (1250 °C). In contrast, air calcination of dried nanoassemblies suspensions, prepared in similar conditions ("PAA-b-PAM−Ba^{2+}−Al_{13}^{7+}" system, $x = 1$, and $r = 2$) yields formation of large BHA crystals, starting from 1150 °C. The higher structure crystallization temperature observed in argon originates from the high interpenetration of PAA and presumably PAM moieties into the nanosized inorganic cores. Indeed, the carbon resulting from the transformation of these oligomers under argon heat treatment, intimately mixed with Ba^{2+} and Al_{13}^{7+}, delays the BHA structure crystallization. Higher temperature of 1250 °C is thus required to promote diffusion and structure crystallization of the BHA, resulting in primary crystal size on the order of 200 nm determined from XRD investigation.

Removal of carbon from the BHA crystals−carbon mixtures is achieved by performing subsequent oxidative post-treatment in air at a much lower temperature, 600 °C. Comparative observation of XRD diffractogramms before and after 600 °C air heat treatment shows no significant BHA primary crystallite growth. TEM images of the air-calcined samples show presence of discrete, ultrafine BHA crystals in association with some loose-packed aggregates. Better individualization of the BHA crystals was obtained by ball milling of the loose-packed aggregates using 0.25 mm Al_2O_3 balls. TEM images of BHA heat-treated successively in 1250 °C for 6 h in Ar, 600 °C for 2 h in air, and ball milled show highly crystallized, nonaggregated 250 nm mean size crystals (Figure 4). Energy dispersive X-ray spectroscopy (EDS) studies of the chemical composition performed on individual nanoplatelets using a small probe size of 0.7 nm x 0.7 nm clearly show the presence of Ba and Al in the BHA stoichiometric ratio, demonstrating that these particles are fully identified

(25) Lee, J. H.; Beaucage, G.; Pratsinis, S. E.; Vermury, S. *Langmuir* **1998**, *14*, 5751.
(26) Beaucage, G. *J. Appl. Crystallogr.* **1996**, *29*, 134.

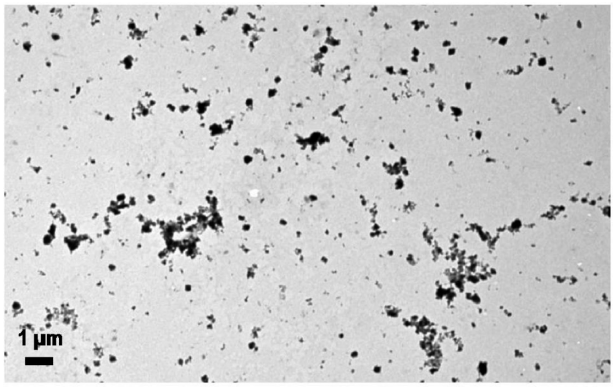

Figure 4. TEM image showing presence of nonaggregated, ultrafine BHA crystals displaying a size of about 250 nm. The sample was prepared in the system "Al_{13}^{7+}−Ba^{2+}−PAA-b-PAM" $r = 2$, $x = 1$, $\Phi_{vBHA} = 0.025$. The sample was calcined successively at 1250 °C in Ar and 600 °C in air.

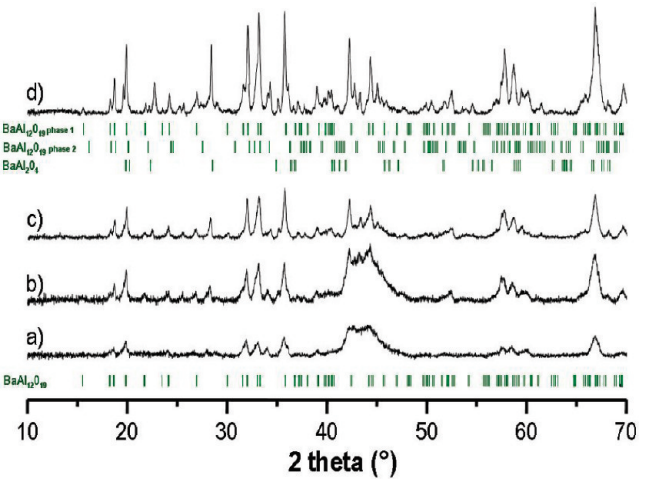

Figure 5. XRD patterns of BHA−carbon mixtures synthesized at different Φv_{BHA}: (a) 0.025, (b) 0.0375, and (c) 0.05 after calcination at 1300 °C under argon showing a better BHA primary crystallite growth inhibition with decreased Φv_{BHA} values. (d): Corresponding X-ray pattern of pure BHA sample after calcination at 600 °C under air, $\Phi v_{BHA} = 0.0375$, 1300 °C. For each pattern, Bragg peaks of various phases are reported.

as BHA crystals. All these observations demonstrate size control in the range of 100−300 nm for barium hexaaluminate crystals in which structure crystallization requires heat treatment at a temperature as high as 1300 °C.

III.2. Synthesis of Ultrafine BHA and BAM Particles Formed from $Al(OH)_3$ Colloids Dispersed onto a Transient Carbon Matrix. *BHA Precursor*. The fabrication of ultrafine BHA crystals, displaying various morphology and size, involves manipulating various parameters such as the Ba/Al ratio, Ba^{2+} distribution, and $Al(OH)_3$ interparticle distance into the carbon−BHA precursors. The control of growth and aggregation rates during the high-temperature diffusion step has been achieved through fine-tuning the $Al(OH)_3$ interparticle distance, d_{Al-Al}, which can be determined from the BHA volume fraction in the carbon−BHA mixtures, Φv_{BHA} = (volume BHA)/[(volume BHA) + (volume carbon)] and the surface area of the carbon matrix. Various high surface area carbons were investigated displaying surface areas in the range of 1800−2300 $m^2\ g^{-1}$. Because this high surface area mainly originates from micropores, a crucial parameter for the selection of the high surface area carbon matrix governing the 4 nm $Al(OH)_3$ nanoparticle dispersion is the surface area displayed by mesopores with diameter distribution ranging from 1.5 to 10 nm. Homogeneous distribution of the Ba^{2+}−$Al(OH)_3$ colloids into the high surface area carbon matrix was achieved from suspensions preadjusted at pH 4.5, optimum conditions for developing highly repulsive $Al(OH)_3$ interparticle interactions.

BHA Structure Crystallization and Preparation of Individual, Ultrafine BHA Particles. Using a carbon matrix, exhibiting a high mesoporous surface area of about 200 $m^2\ g^{-1}$ (PICA), XRD investigation demonstrates that crystals of BHA formation were achieved in the high temperature range of 1100 °C < T < 1350 °C for Φv_{BHA}, $0.025 < \Phi v_{BHA} < 0.05$ (Figure 5). This corresponds to calculated $Al(OH)_3$ interparticle distances of 33 nm < d_{Al-Al} < 66 nm assuming a homogeneous distribution of the $Al(OH)_3$ nanoparticles onto the carbon mesoporous surface. Another important parameter to control is the Ba/Al ratio. In our procedure, the homogenenous distribution of $Al(OH)_3$ nanoparticles onto the high surface area carbon matrix was achieved through the slow evaporation at 80 °C of an aqueous dispersion containing the carbon matrix, $Al(OH)_3$ nanoparticles, and dissolved $Ba(NO_3)_2$ in the desired Ba/Al ratio. In these conditions, and employing an aqueous dispersion adjusted at pH 4.5, our optimal conditions promoting fabrication of ultrafine BHA crystals were obtained with a Ba/Al ratio in the range of $0.09 < Ba/Al < 0.12$, a value slightly larger than the BHA stoichiometric ratio.

Carbon−BHA mixtures containing BHA crystals were thus prepared at $\Phi v_{BHA} = 0.0375$, Ba/Al = 0.095, at 1300 °C. Larger Φv_{BHA} values, $\Phi v_{BHA} > 0.04$, result in formation of larger BHA crystallized domains as revealed from full width at half-maximum (fwhm) determination of X-ray diffraction peaks. In contrast, samples synthesized at lower Φv_{BHA} values, $\Phi v_{BHA} < 0.03$, are composed of a mixture of BHA, $BaAl_2O_4$, and Ba−β Al_2O_3 structures. This illustrates the barrier effect of the carbon matrix toward reactants diffusion. Indeed, using our evaporation−drying procedure, a too small Φv_{BHA} value delimitate nanodomains displaying nonstoichiometric BHA chemical compositions. Regarding the Ba/Al ratio, carbon−BHA mixtures synthesized at lower values than the stoichiometric value (Ba/Al = 0.09) contain additional Al_2O_3 structures, whereas values of Ba/Al > 0.11 yield consistent $BaAl_2O_4$ formation. It should be also noted that the formation of BHA crystals in our carbon−BHA mixtures, based on the Ba^{2+} diffusion into $Al(OH)_3$ nanoparticles, occurs at 1300 °C, a temperature slightly higher than that reported for the citrate process.[17,18] In addition, investigation of the onset of the BHA structure crystallization shows that various Al_2O_3 structures are involved as clearly revealed by XRD patterns recorded on products calcined at intermediate temperatures, 1150 °C < T < 1250 °C, showing the presence of θ Al_2O_3. In comparison with the route involving copolymer micelles, all these observations suggest a different formation

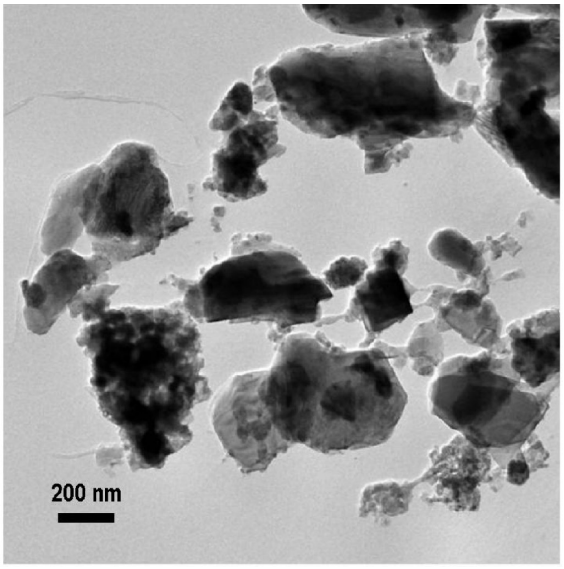

Figure 6. TEM images showing discrete 300 nm mean size BHA crystals heat treated at high temperature, 1300 °C. Scale bar = 200 nm.

mechanism for the BHA crystals with Al_2O_3 nanoparticles acting as nanoreactors.

Production of ultrafine BHA crystals from the BHA−carbon mixtures was achieved through pyrolysis of the inert carbon matrix, performed under subsequent air calcination at 600 °C for 2 h. XRD patterns recorded on products before and after carbon removal exhibit analogous peaks, nevertheless with a better peak resolution for air-calcined products. This confirms that no drastic change of the product characteristics occurs during this pyrolysis step, which has been performed at a much lower temperature. XRD patterns of samples calcined at 1300 °C in Ar and 600 °C in air, clearly show a BHA structure with peaks attributed to the BaO, 6 Al_2O_3 structure (space group $P6_3/mmc$ hexagonal, $a = b = 5.5992$ Å, $c = 22.6743$ Å). More interestingly, for the optimal conditions of achieving the smallest BHA crystallite size ($\Phi v_{BHA} = 0.0375$, 1300 °C for 4 h, 600 °C in air), the XRD patterns show in addition to the BaO, 6 Al_2O_3 phase, the presence of peaks associated to a second BaO, 6 Al_2O_3 phase, but possessing a smaller unit cell size (Figure 5). The Rietveld refinement of corresponding XRD pattern was undertaken, yielding calculated cell parameters of $a = b = 5.5661$, $c = 21.9565$ Å, with reasonable values of χ^2 (5.72) and R_{wp} (7.02). This phase could result from a nonstoichiometric BaO, 6 Al_2O_3 in which formation has been promoted by the slow growth regime involving diffusion of Ba^{2+} into preformed Al_2O_3 nanoparticles. TEM observation of the air-calcined products shows the presence of ultrafine crystals exhibiting platelet morphology and the presence of some loose-packed BHA aggregates (Figure 6). Fine inspection of the TEM images of samples prepared at various Φv_{BHA} confirmed that the loose-packing of the aggregates is promoted by synthesis performed at low Φv_{BHA}, corresponding to highly dispersed $Al(OH)_3$ nanoparticles onto the high surface area carbon matrix. We propose that the observed anisotropic morphology of the ultrafine BHA crystals arise from a BHA crystal formation mechanism operating under a growth regime involving $Al(OH)_3$ nanoparticles. Size monodispersity of the BHA nanoplatelets was improved after ball milling during 1 h using 0.25 mm Al_2O_3 balls. For BHA samples prepared at $\Phi v_{BHA} = 0.0375$, and calcined at 1300 °C for 4 h in Ar and 600 °C in air, a surface area of 50 $m^2\ g^{-1}$ was determined on the dried ball-milled crystals. TEM observations clearly demonstrate the presence of nonaggregated BHA nanoplatelets displaying a 250 nm mean size. An average thickness in the range on 4−10 nm was determined through the fine inspection of TEM images with the presence of some nanoplatelets oriented perpendicular to the observation plane. Local chemical composition, investigated by EDS, was performed on individual platelets using a smaller probe size of 0.7 nm x0.7 nm. This more localized chemical analysis clearly indicates the presence of Ba and Al in the BHA stoichiometric ratio, demonstrating that these platelets could be fully identified as BHA crystals.

Transposition to Ultrafine BAM Crystals. Our synthetic procedure was successfully used to the preparation of $Ba_{0.9}Eu_{0.1}MgAl_{10}O_{17}$, (BAM:$Eu^{2+}$) individualized ultrafine phosphors. Because of the large number of cations involved in the fabrication of BAM:Eu^{2+} phosphors, we slightly modified our procedure for the fabrication of the carbon/BAM:Eu^{3+} precursor. In order to achieve a better chemical homogeneity of the distribution of the various cations into the carbon−BHA precursors, evaporation−drying of the suspension containing $Al(OH)_3$ nanoparticles, dissolved $Ba(NO_3)_2$, $Mg(NO_3)_2$ $Eu(NO_3)_2$, and carbon matrix was performed from a ($EtOH-H_2O$) solvent mixture and under vacuum at 80 °C. As a result, XRD patterns of carbon−$Al(OH)_3$−$Ba(NO_3)_2$, $Mg(NO_3)_2$, and $Eu(NO_3)_3$ dried mixtures do not exhibit any peak attributed to metal nitrate salts, suggesting a high chemical homogeneity. Using this modified procedure, slightly lower Φv_{BAM} and temperature calcination ($\Phi v_{BAM} = 0.025$, $T = 1250$ °C) than those required for BHA crystal formation were observed for the synthesis of BAM:Eu crystals. To develop the luminescence property of these BAM:Eu crystals, we performed am additional heat treatment under Ar, 3.9% H_2 allowing the reduction of $Eu^{3+} \rightarrow Eu^{2+}$ at 750 °C for 2 h on samples after successive calcinations at 1250 °C in Ar and 600 °C for 2 h in air. No significant change of the XRD patterns recorded on the samples before and after the reduction step was observed. In contrast to the BHA X-ray patterns which display two polymorphs, a unique BAM structure was identified resulting in less overlapping of the BAM peaks. A primary crystallite size of 180 nm for the (103) reflection using the Scherrer model was determined for BAM:Eu^{2+} nanocrystals heat treated at 1250 °C. TEM images performed on the ball-milled samples show the presence of highly crystallized, nonaggregated, ultrafine phosphors displaying platelet morphology (Figure 7) with a mean size of about 200 nm. As for the ultrafine BHA crystals, the low contrast exhibited by the platelets on the TEM images suggests a low thickness of the phosphors. This is

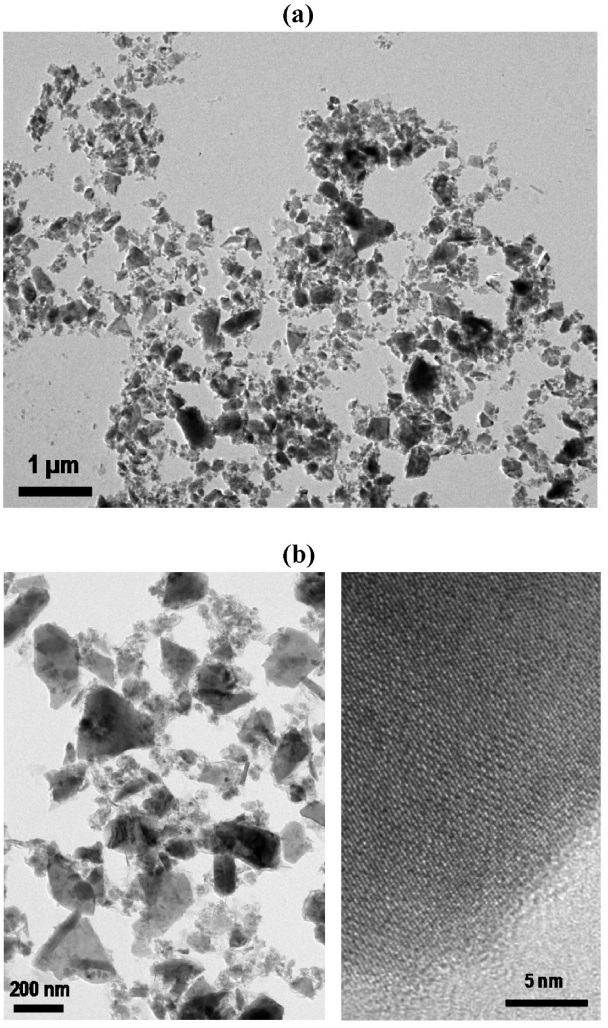

Figure 7. TEM images of BAM:Eu^{2+} showing (a) ultrafine, nonaggregated phosphors at low magnification, scale bar = 1 μm; (b) platelet morphology of the ultrafine BAM:Eu^{2+} particles, scale bar = 200 nm. Insert: High magnification image showing reticular planes demonstrating crystallization of the platelets. Scale bar = 5 nm.

confirmed by the high surface area of 70 $m^2\ g^{-1}$ determined on this product. Additional evidence of the structure crystallization of our phosphors is given by the luminescence properties of these ultrafine BAM:Eu^{2+} phosphors. The emission spectra excited at 320 nm show the highest blue emission intensity at 453 nm and a second minor peak at 516 nm, which corresponds to the green emission of he BAM.

Size and Morphology Control of the Ultrafine BHA and BAM Crystals. Our approach to fabricate ultrafine refractory complex aluminate crystals is based on the inhibition of growth and aggregation mechanisms, achieved with the presence of transient carbon spacers during the high-temperature crystallization step. Indeed, control experiments performed without the use of carbon demonstrated that highly compact aggregates possessing large crystallite size were obtained through these current synthesis methods as revealed by XRD and TEM investigations. Subsequent ball milling of these large crystals produce, as expected, particles displaying a mean size around 350 nm, larger than those produced by the synthetic methods developed in this paper. More importantly, morphology control of refractory complex oxide crystals was obtained by tailoring the distribution of the various cations onto a carbon matrix. A growth regime for the fabrication of ultrafine refractory crystals was designed involving homogeneous dispersion of colloids of the main cation [$Al(OH)_3$ colloids] combined with an homogeneous distribution of the others cations (Ba^{2+}, Mg^{2+}, Eu^{3+},..) onto the carbon matrix. Morphology control of the ultrafine crystals was thus achieved through Φv_{BHA} optimization, this parameter dictating the diffusion length of the Ba^{2+} (and optionally Mg^{2+}, Eu^{3+}) cations. In addition, we can note that for the two methods we do not observe fabrication of smaller size BHA nanocrystals by multiplying nucleation centers with an increase in the BHA volume fraction, Φv_{BHA}. In contrast, the lowest BHA primary crystal size is achieved with low Φv_{BHA} values corresponding to large distances between the BHA precursor nanoreactors. All these observations confirm the inhibition of BHA crystals growth by the carbon matrix and a diffusion-controlled mechanism for the ultrafine BHA crystal formation.

IV. Conclusions

In conclusion, a novel method for the size control of nonaggregated, ultrafine particles of refractory complex aluminates was developed for the synthesis of $BaAl_{12}O_{19}$ (BHA) or $Ba_{0.9}Eu_{0.1}MgAl_{10}O_{17}$ (BAM) crystals in which structure crystallization requires temperatures as high as 1300 °C. Control of morphology of these refractory complex aluminates displaying nanoplatelets morphology was achieved via the tailoring of high-temperature diffusion lengths of the various cations involved in the formation of these ultrafine refractory crystals. Future improvements for achieving smaller crystal size will include use of a carbon matrix displaying higher mesoporous surface area or synthesis of more chemically homogeneous precursors, which could be ideally described as core−shell nanoparticles composed for instance of a $Ba_{1-x}Eu_xMgCO_3$ shell and $Al(OH)_3$ cores. Further investigation would extend this method for the synthesis of other ultrafine refractory complex oxides crystals.

Acknowledgment. This work was supported by the Agence Nationale pour la Recherche, ANR, France. This work was completed through the PNANO−SPOT project, involving the collaboration of LPMC−Ecole Polytechnique, Rhodia, and Saint Gobain companies. The authors thank Prof. J.P. Boilot and T. Gacoin, Ecole Polytechnique, France, for discussions and providing luminescence data.